ASCE
American Society of Civil Engineers

May 2007
Volume 133, Number 5

ISSN 1090-0241
CODEN: JGGEFK

Journal of Geotechnical and Geoenvironmental Engineering

Technical Papers

contents continue on back cover

GEO INSTITUTE
The Geo-Institute

Laboratory Rainfall-Induced Slope Failure with Moisture Content Measurement

Adrin Tohari[1]; Makoto Nishigaki[2]; and Mitsuru Komatsu[3]

Abstract: The development of a physically based warning system for rainfall-induced slope failures requires a comprehensive understanding of the failure process. A set of laboratory-scale soil slopes was subjected to instability, through three different modes of raising water level, to clarify the process of failure initiation. Hydrologic responses of the model slopes to the saturation process were recorded by volumetric soil moisture content sensors. The results of model tests show that failures of the model slopes were essentially initiated by the development of an unstable area near the slope toe, upon the formation of the seepage area, with shallow noncircular sliding being the dominant failure mode. The volumetric moisture content of the slope region where localized failures initiated was noted to reach a nearly saturated value. However, the major portion of soil slopes involved in overall instability was still in an unsaturated condition. Based on the observed moisture content response of the model slopes, a concept for prediction methodology of rainfall-induced slope failures is introduced.

DOI: 10.1061/(ASCE)1090-0241(2007)133:5(575)

CE Database subject headings: Laboratory tests; Landslides; Moisture content; Predictions.

Introduction

Rainfall-induced slope failures are reported to occur during or immediately following periods of intense or prolonged heavy rainfall. These slope failures most frequently occur on natural slopes in a variety of materials, including residual and colluvial soils, in tropical or subtropical climates. There is also some field evidence that cut slope and slope embankment may be potentially prone to this type of slope failures (e.g., Harp et al. 1996; Baum and Chleborad 1999). Field evidence indicates that these slope failnres are generally of small volume, typically involving shallow sliding (less than 2 m deep) above the groundwater table on steep soil slopes of 30 to 50° (Johnson and Sitar 1990; Anderson and Thallapally 1996; Baum and Chleborad 1999; Rahardjo 1999). They may initiate on concave and planar slopes (Wieczorek 1987). Although relatively small volume, these occurrences claim untold numbers of human lives and cause great economic losses every year in many parts of the world.

Understanding of mechanisms and conditions leading to the initiation of rainfall-induced slope failures has been generally gained from field measurements and laboratory strength tests. From the results of field measurements, it is generally accepted that the rapid rise of rainfall-induced pore-water pressure is critical to the initiation of slope failures (Johnson and Sitar 1990). It is typically observed that significant build up in positive pressure heads is generated in an area low on the slope (Sitar et al., 1992; Anderson and Thallapally 1996); however, the mechanism of pore-pressure generation differs from site to site depending on the site hydrology, topography and soil properties (Sitar et al. 1992). In Singapore and other tropical countries, the effect of reduction in soil suction on soil shear strength has been accounted for in explaining the mechanism of rainfall-induced slope failure in residual granite soil slopes (Rahardjo 1999). Meanwhile, laboratory shear tests under the field stress path have been used to study strength parameters for analysis of the potential for the initiation of rainfall-induced debris flow failures (Sitar et al. 1992; Anderson and Sitar 1995). The results of these studies suggest that these types of slope failures involve drained initiation along a stress path characterized by decreasing effective stress and nearly constant shear stress.

While previous studies have led to the understanding of mechanisms and conditions leading to the initiation of rainfall-induced slope failures, there have been few investigations of the actual process of failure initiation. Until now, the initiation process has remained unclear. The effects of soil hydrologic properties, soil fabric, slope morphology, and other unknown factors may control the process leading to the initiation of slope failures. Thus, it seems highly important to clarify the initiation process, because this clarification can lead to a comprehensive understanding of slope failure processes, which is essential for performing quantitative analysis of failure hazards, developing physically based forecast systems for failure occurrences, and taking subsequent appropriate preventive measures to mitigate these hazards.

In previous studies of rainfall-induced slope failure, some efforts have also been made to develop a pre-event warning system.

[1]Researcher, Research Centre for Geotechnology-Indonesia Inst. of Sciences, Jl. Sangkuriang, Bandung 40135, Indonesia. E-mail: adrin@cbn.net.id

[2]Professor, Dept. of Environmental and Civil Engineering, Okayama Univ., Tsushimanaka 3-1-1, Okayama 700-0082, Japan. E-mail: makoto@gw.civil.okayama-u.ac.jp

[3]Assistant Professor, Dept. of Environmental and Civil Engineering, Okayama Univ., Tsushimanaka 3-1-1Okayama 700-0082, Japan. E-mail: mkomatsu@cc.okayama-u.ac.jp

Note. Discussion open until October 1, 2007. Separate discussions must be submitted for individual papers. To extend the closing date by one month, a written request must be filed with the ASCE Managing Editor. The manuscript for this paper was submitted for review and possible publication on May 15, 2001; approved on January 6, 2006. This paper is part of the ***Journal of Geotechnical and Geoenvironmental Engineering***, Vol. 133, No. 5, May 1, 2007. ©ASCE, ISSN 1090-0241/2007/5-575–587/$25.00.

This subject received increasing interest from researchers in many different fields of study; the subject of slope failure prediction is very complex and requires integrated knowledge of climate, geology, slope morphology, hillslope hydrology, and soil strength. Numerous attempts have been made to correlate rainfall data with the occurrence of landslides for developing pre-event warning systems (e.g., Caine 1980). However, the preliminary research of Church and Miles (1987) indicates that rainfall intensity cannot be used as the sole basis of a slope failure warning system. Other factors such as rainfall characteristics, antecedent precipitation, geologic, and topographic conditions must also be accounted for in the occurrence of landslides (Wieczorek 1987; Keefer et al. 1987; Reneau and Dietrich 1987). Sammori et al. (1996) investigated the effect that soil thickness may have on slope failure initiation, and pointed out that knowledge of soil thickness and hydraulic properties of soils can be used to predict the time of a failure event. However, this approach applies only to soil slopes with uniform thickness.

Recently, in attempts to develop a predictive warning system for rainfall-induced slope failures, a number of studies have focused on monitoring the hydrologic response of a soil slope under the effect of infiltration. Most of these involved the monitoring of pore-water pressures in saturated and unsaturated conditions (e.g., Johnson and Sitar 1990; Anderson and Thallapally 1996; Rahardjo 1999; Fannin and Jaakkola 1999). However, the present-day devices for measuring in situ pore-water pressures, such as standard piezometers and tensiometers, still have some practical limitations on their performance and reliability. Some limitations of the piezometer include; the potential for clogging of the filter, and hydrodynamic time lag in response to changes of groundwater pressure (Abramson et al. 1996; Fannin and Jaakkola 1999). The standard tensiometers, like the vacuum gauge style, lack in response time and accuracy (Fannin and Jaakkola 1999). These drawbacks obviously hinder the prediction of a particular failure hazard; and thus, there is a need for a reliable and effective approach to measuring the hydrologic condition during rainwater infiltration, for the purpose of predicting the occurrence of slope failures.

From a hydrologic point of view, the hydrologic response of soil slopes to rainfall can also be characterized by a change in the moisture content of the soil. More recently, a number of nonradioactive and simple methods for measurements of volumetric soil moisture coutent has been developed based on the dependence of the dielectric constant on the volumetric moisture content of a soil. In principle, these methods employ electromagnetic pulses to quantify the soil moisture content. The methods include: Time Domain Reflectrometry (Topp et al. 1980; Whalley 1993), frequency domain reflectrometry or capacitance method (Ji et al. 1996), and amplitude domain reflectrometry or impedance method, e.g., ThetaProbe (Miller and Gaskin 1996), and are capable of performing long-term measurement, and indicating the saturated and unsaturated conditions of soils. They have had extensive application in agricultural and geoenvironmental fields of study with limited use in geotechnical fields of study (e.g., Coe et al. 2000; Teysseire et al. 2000). Some studies have also focused on evaluating the performance of a variety of soil moisture sensors, including dielectric sensors (Hanson 1999; Charlesworth 2000). Of those dielectric seusors, ThetaProbes (Delta-T devices 1996) have been proved most consistently accurate over a wide range of soil textures (Hanson 1999), and have been applied in a number of field projects (e.g., Miller and Gaskin 1996).

This paper presents the results of a series of laboratory experiments on rainfall-induced slope failures. The experimental program consists of detailed observations of failure initiation process, failure modes, and changes in soil moisture content during failure initiation. The changes in the initial hydrologic condition, and the instability were induced in model slopes through three different modes of raising water level. The specific objectives of this study were to (1) document and clarify the failure initiation process; (2) evaluate the critical influence of seepage area on failure initiation; and (3) develop a concept of moisture content-based prediction methodology for rainfall-induced slope failures. *ThetaProbe* sensors were used to monitor changes in volumetric soil moisture content because of their practicality, fast response time and accuracy.

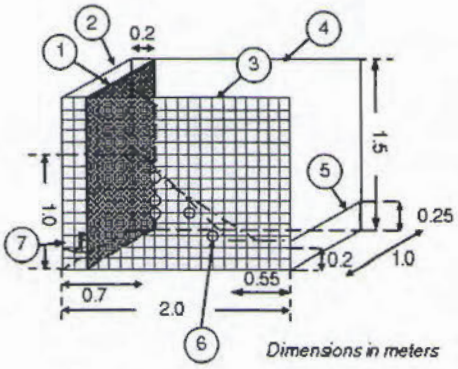

Fig. 1. Outline of slope failure tank, slope profiles (dotted–dashed line), locations of moisture sensor (circle) and initial water table

Properties of Experimental Soil

Two different sandy soils, namely, river sand and residual granite soil were used to construct a number of homogeneous experimental slopes in this study. The effective particle size (D_{10}) and uniformity coefficient (D_{60}/D_{10}) of the river sand are 0.175 and 7.14 mm, respectively. The residual granite soil has an effective particle size and uniformity coefficient of 0.157and 4.63 mm, respectively. Tests of specific gravity produced a value of 2.69 for both soils. The maximum dry density, from the standard Proctor test, is 1,800 kg/m^3 at an optimum water content of 14.5% for the river sand and 2,010 kg/m^3 at an optimum water content of 11.8% for residual granite soil. The saturated hydraulic conductivity (k_s) obtained from constant head permeability tests using a rigid wall permeameter on the river sand was 6.4×10^{-2} cm/s at void ratio of 0.82 and on the residual granite soil was 7.2×10^{-3} cm/s at void ratio of 0.52. Shear strengths of both soils were obtained from conventional isotropically consolidated drained triaxial compression (ICD) tests. The tests show that the river sand and residual granite soil are cohesiouless with an angle of internal friction of 50 and 37°, respectively.

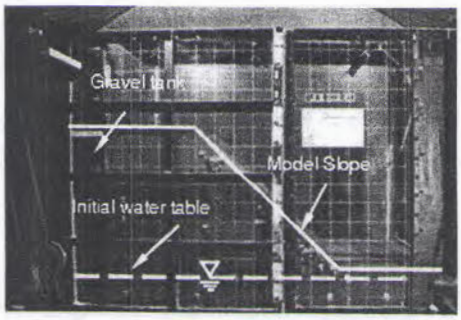

Fig. 2. Position of gravel tank with respect to the model slopes in Experiments 1 and 2 (dashed-white line indicates the initial water level)

Experimental Apparatuses

Model Slope Tank

The experiments were conducted in a metal tank with maximum dimensions of $2.0 \times 1.0 \times 1.5$ m, as shown schematically in Fig. 1. An acrylic board, 20 mm thick, was installed on one side of the tank for allowing the simple installation of the instrument system and observation of the deformation process. To generate an impervious boundary at the end of the model slope, a 10 mm acrylic board, 25 cm in height, was secured at the slope end. The tank structure was rigidly constructed to minimize deflection.

A thin layer of sand was glued to the floor of the tank to create friction and to inhibit direct sliding of the slope base along the soil/floor interface. Meanwhile, no artificial friction was created on the surface of the sidewall to prevent the model slope from sliding along the wall. For the installation of instruments, five holes, each 41 mm in diameter, were drilled in the observation window at designated points (Fig. 1). Several tracer injection holes, 3 mm in diameter, were also drilled into the observation window at 10 cm spaces and resealed with silicon sealant.

Detachable Gravel Tank

A detachable coarse gravel-filled tank, 20 cm thick with porous sheet outlets, was installed in the slope failure tank to generate the lateral inflow of water from a constant head tank into the model slopes in Experiments 1 and 2 (Fig. 2). The gravel tank prevented internal erosion within the soil owing to scouring during the increase in water level.

Slope Profile and Soil Placement

In the current study, straight and homogeneous slope profiles were used in all experiments, with the geometry of model slopes not inhibiting and confining the development of failure surface, as well as the occurrence of slope failures. The slope profiles did not include any other factors, such as soil heterogeneity, hydraulic conductivity contrasts and topography features (e.g., hollows or swales), as the influences of those factors on the process of failure initiation were beyond the scope of the current study.

Four experimental soil slopes were constructed by placing wet soils in a series of horizontal layers 50 mm thick to the full width of the tank. The wet soils were prepared by mixing up dry soils thoroughly with water to give the prescribed water content using a mixer. For the first three experiments, the river sand with a uniform water content of 5% was used to construct initially dry slope profiles. For Experiment 4, the residual granite soil was placed at its optimum water content of 11.8% to construct an initially wet model slope. Light compaction was applied to each soil layer using a wooden tamper to give slight apparent cohesion. It took about 6 h to complete the construction. Upon the completion, the slope tank was covered with a plastic sheet to minimize moisture content loss due to evaporation, and was allowed to reach equilibrium moisture content condition for 12 h, before commencing the experiments.

The profiles of each model slope are presented in Fig. 3. The slopes were 0.75 m high and 1.0 m wide. The soil thickness at the slope base was 0.25 m. The slope angle of 45° was chosen for the first three experiments, and the 32° slope angle was used in the residual granite soil slope. These slope angles were considered to represent the inclination of natural soil slopes at which shallow slope failures are common (e.g., Wieczorek 1987; Rahardjo 1999).

The average dry density of the profiles were then determined from the total density and average placement water content, and were subsequently used to estimate average relative density and void ratio for each slope profile, as presented in Table 1. It is clear from this table that although placement water content for the river sand slopes were identical, the compaction had given rise to different relative density, with the model slope for Experiment 3, apparently, being very densely placed.

Experimental Instrumentation

Upon the introduction of water level rise, the moisture content within the slope would change during slope wetting. To monitor the changes of volumetric soil moisture content with time

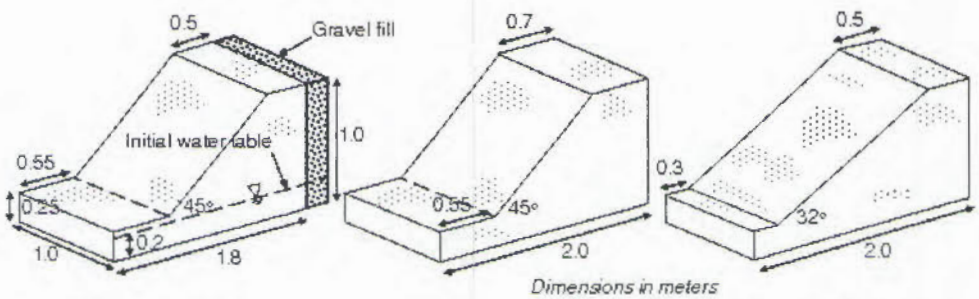

Fig. 3. Profiles of each slope model

Table 1. Properties of Experimental Slopes

Experiment number	Soil used	α (degrees)	ρ_d (kg/m^3)	D_r (%)	e/n	Average θ_i Base	Average θ_i Middle	θ_s[a]
1	River sand	45	1.43	53.10	0.88/0.46	0.46[b]	0.07	0.46
2	River sand	45	1.41	49.86	0.91/0.48	0.48[b]	0.07	0.48
3	River sand	45	1.48	60.81	0.82/0.45	0.08	0.08	0.45
4	Residual granite soil	32	1.78	61.59	0.52/0.34	0.27	0.20	0.34

[a]Calculated from void ratio or porosity.

[b]Values after introduction of initial water level.

throughout the experiment, the model slopes were instrumented with four ThetaProbe (TP) Type ML1 (delta devices model) moisture sensors. These sensors have a response time of less than 0.5 s, and are able to measure volumetric moisture content (V_w/V) within the range of 0 to approximately 0.5 m^3 m^{-3}, with typical errors of at least +0.02 m^3 m^{-3} when calibrated for a specific soil, and 0.05 m^3 m^{-3} otherwise. Although they offer consistent accuracy, the performance of the sensors is affected by some factors, such as soil salinity and the presence of an air pocket around the sensing head (Delta-T devices Ltd., 1996).

Prior to their installation, the four *ThetaProbe* sensors were calibrated with residual granite soils and river sand. The calibration results were fitted by fifth-order polynomial with the measurement errors of output voltage within 0 to 0.02 V, as shown in Fig. 4. The moisture sensors (TP1-TP4) were then inserted into the model slopes at certain points through the holes in the observation window, with care being taken to avoid the presence of air pockets around the rods. Silicon grease was also applied on each sensor body to secure a good fitting between the sensor body and the insertion holes. Upon the completion of insertion, they were connected to a microcomputer-based data acquisition system, and were logged at approximately 60 s intervals. The configuration of the moisture sensors for each experiment is shown in Fig. 5, and the setup of the moisture sensor in the soil is shown in Fig. 6.

Rainfall Simulator

A rainfall simulator was set approximately 1.0 m above the model slopes to induce the change in volumetric moisture content and instability in the model slope in Experiments 3 and 4. The simulator was designed to produce an effective rainfall intensity of approximately 10 cm/h. To limit the fluctuation of water pressure, in the water supply, the amount of water flowing into the sprayer arms was carefully controlled, and monitored through a flow meter to maintain rainfall at the prescribed intensity.

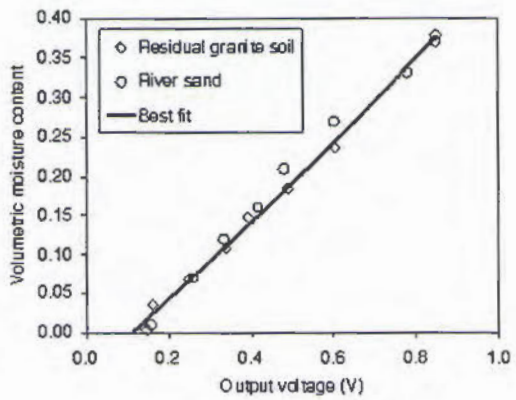

Fig. 4. Calibration curve for ThetaProbe sensors

Photography

A video camera was set up in front of the slope face to give a better view and complete record of the saturation process, failure initiation and movement. A 35–70 mm auto focus camera was used to record the flow lines, slope profile before and after failure, and the displacement of the sliding block.

Experimental Details

The first two experiments focused on the effect of different rates of raising water levels on the failure process and change in moisture content. The rate of water level rise within the slopes was controlled by a constant head tank. In the first experiment, a slow rise of water level was introduced by raising the constant head

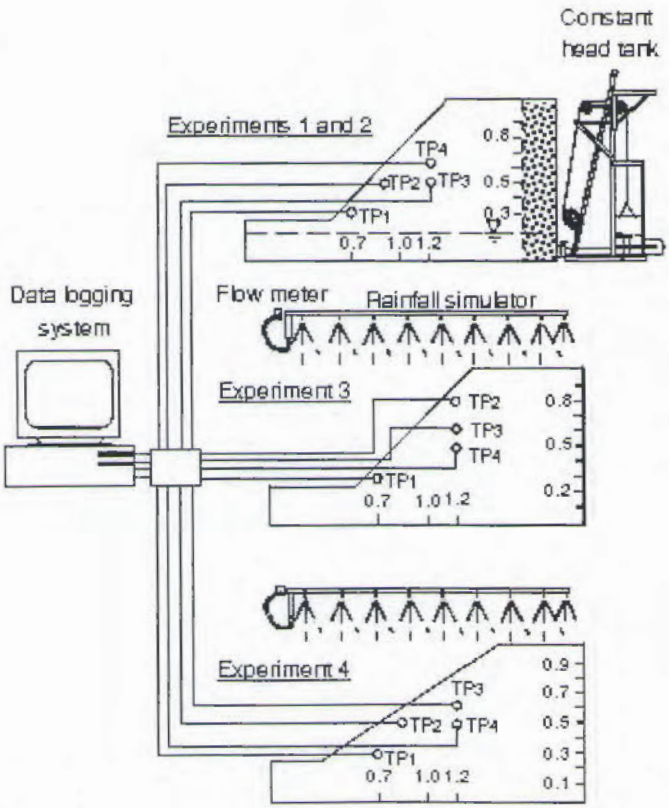

Fig. 5. Overview of instrumentation and data logging system (elevation in meters)

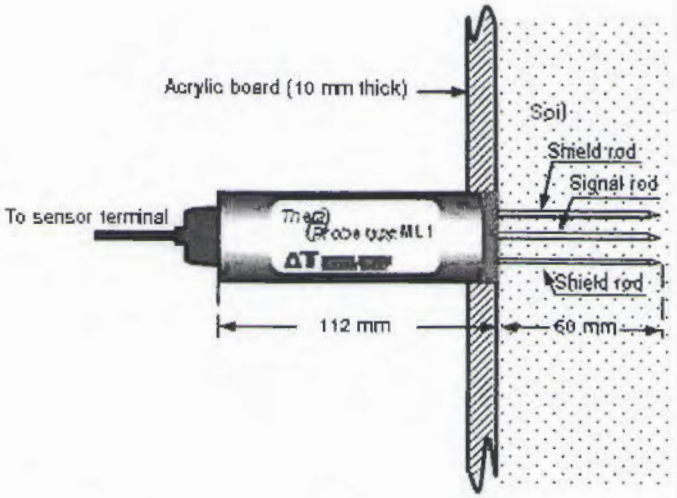

Fig. 6. Setup of the *ThetaProbe* sensor in the model slopes (not to scale)

tank level 5 cm every hour up to a maximum height of 65.5 cm. At each step, the flow of water within the slope was allowed to achieve a steady-state condition before the introduction of the subsequent rise in water level. The second experiment examined a condition of rapid water level rise by raising the constant head tank level in steps at a rate of 5 cm/min up to a height of 60 cm. Prior to these two experiments, a water level of about 20 cm, was introduced to produce an initial water level across the base of each slope from the constant head tank, and to prevent a premature sliding on soil/base interface (Fig. 2). This introduction of the initial water level was considered eliminating the seepage pressures acting on soils across the base of the slope during the experiments.

The effects of rainwater infiltration on the failure process and moisture content change within the slope were investigated in the last two experiments. In these two experiments, heavy rainfall with intensity of approximately 10 cm/h was simulated. The accumulation of entrapped air within the soil slopes was reduced by opening a valve at the end of the tank, during infiltration until the wetting front touched the base of the tank. Because the simulated rainfall would introduce surface erosion and formation of gullies, the entire surface of the model slope was covered by a colorless plastic net with 1 mm meshes. Since the plastic net was not embedded in the soil, the use of the plastic net would not deter the process of the downward percolation of rainwater towards the bottom of the tank, and would not exert additional shear strength to the soil. At the commencement of each experiment, blue tracers

Table 2. Salient Features at Toe Saturation and Failure

Experiment number	Time for toe saturation (min)	Water level at toe saturation (cm)[a]	Time to failure
1	73	28	Varied from 1 to 15[b]
2	11	35	6[c]
3	54	34	36[c]
4	420	27.5	450[c]

[a]Values under the slope crest.

[b]Values after each stage of water level rise.

[c]Values after the first toe saturation.

were injected through the injection holes to visualize the flow lines within the slope profile and to trace the failure lines in unsaturated zone of the model slopes.

Results of Model Tests

Detailed Observation of Failure Process

Prior to the initiation of slope failures, the ingress of the wetting front introduced significant increases in water level, within the slope, and the development of seepage area at the slope toe. The length of time to reach full water saturation at the toe, in each experiment, is tabulated in Table 2; and the factors controlling the saturation were essentially the mode of raising the water level, and the hydraulic of conductivity the model slopes.

In the first two experiments, the infiltration of the saturated wetting front increased the initial water level across the base of the slope, producing a water table with a gradient going directly toward the slope surface. For Experiments 3 and 4, the process of saturation began with rainwater percolating downwards from the entire slope surface toward the bottom of the tank. In Experiment 3, according to the tracer flow patterns, saturated area started to form at the slope toe area, while the advancement of saturated wetting fronts was still in progress along the base of the tank, causing a small mound of water table to form inside the model slope. As a result, the model slope had the water table sloping toward the slope surface, as well as in the opposite direction [for example, at $t=80.3$ min in Fig. 7(a)]. Some water started to seep out of the slope toe, while the water table still developed and rose across the bottom of the slope. The water then flowed toward the slope, allowing the growth of seepage areas above the slope toe.

In Experiments 2 and 3 in particular, toe saturation and seepage areas were observed to develop more rapidly on the side closest to the metal wall. This indicated that saturated wetting

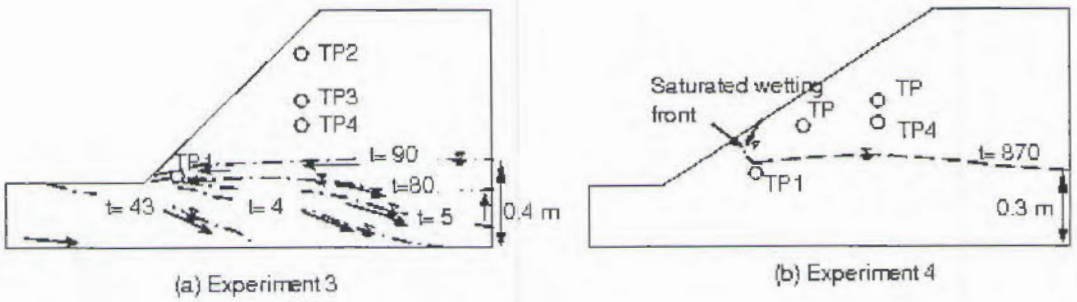

Fig. 7. Development of water table with time within the model slopes (time t in minutes)

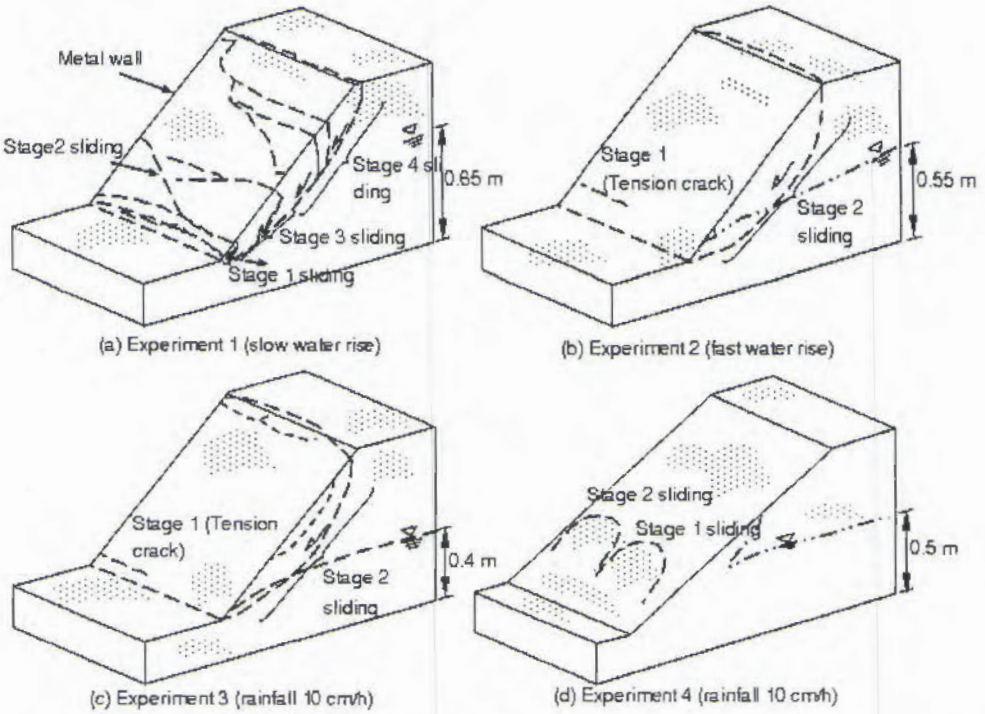

Fig. 8. Overall failure sequence with the traces of failure lines and the corresponding water table level in each model slope

fronts infiltrated more readily along the soil/wall interface, probably due to the presence of large pores along the interface. Consequently, with the absence of friction along the sidewalls, earlier failures were observed to commence on the side adjacent to the walls.

In Experiment 4, the advancement of saturated wetting fronts within the slope profile failed to be fully perceived, because of the prolonged existence of entrapped air in some slope sections adjacent to the observation window. However, on account to the lower hydraulic conductivity, the saturated zone was likely to advance more readily to the near-surface soil than across the base of the slope [Fig. 7(b)].

The details of the failure process obviously varied with each experiment and need to be interpreted in relation to the mode of rising water level. The three-dimensional nature of the failure process in each experiment is systematically shown in Fig. 8.

In Experiment 1, the introduction of slow rise in water level from the constant head tank resulted in the initiation of different stages of failure. The appearance of some localized tension cracks, in the vicinity of the toe area, was concurrent with the first appearance of seepage at the toe when the head tank level was raised to 40 cm. As the head tank level increased to 45.3 cm, the seepage area increased, and consequently, shallow slides occurred in the vicinity of the slope toe [Stage 1 in Fig. 8(a)]. The process of the failure initiation involved the propagation and interconnection of crack tips. Sand slurry was formed around the toe, as seepage water was absorbed into the failed soil mass. The commencement of Stage 2 failure did not occur until the water level in the constant head tank increased to 49.5 cm. A distinct, localized shallow slide then occurred adjacent to the metal plate wall. Two minutes after raising the head tank level to 55.5 cm, a localized shallow slide was observed adjacent to the observation window [Stage 3 in Fig. 8(a)]. The seepage water emerged through the lower part of the failed soil mass. The accumulation of previous sand debris at the toe apparently prevented the further movement of the failed mass in Stages 2 and 3. Raising the water level in the constant head tank to 60.5 cm did not precipitate failure in any part of the slope mass, but resulted in the development of lateral cracks across the uppermost portion of the slope. The seepage area was formed much further from the original toe, and more sand slurries were formed at toe area. A subsequent increase in the constant head tank level to 65.5 cm then caused the movement of the whole unsaturated upper portion of the slope [Stage 4 in Fig. 8(a)], pushing the previously failed sand onto the sliding surface formed by earlier stages of failure.

In Experiment 2, following toe saturation and the growth of seepage area, a tension crack formed at the area just above the saturated toe close to the metal wall, indicating the initiation of toe failure [Stage 1 movement in Fig. 8(b)]. At this stage of movement, the water level in the gravel tank had already risen to 55.2 cm. A few seconds later, the rapid sliding of a slab of sand about 20 cm thick, comprising the whole slope surface occurred [Stage 2 in Fig. 8(b)]. The water level in the gravel tank was noted to increase to 55.4 cm. The movement of the slab brought about the closure of the tension crack formed in the Stage 1 movement without inducing a significant displacement of the toe saturated sand mass.

In Experiment 3, the first appearance of the water table at the base of the slope caused the formation of a lateral crack across the crest of the slope 45 min after the commencement of the experiment, probably due to the loss of moisture tensions in the soil. Subsequent to the appearance of seepage area at the toe, a tension crack formed adjacent to the metal wall a few centimeters above the slope toe, indicating the initiation of toe failure [Stage 1 in Fig. 8(c)]. This tension crack was observed to grow with the further extent of seepage area uphill resulting in a movement in which the whole slope surface, about 15 cm thick, slid quite rapidly [Stage 2 in Fig. 8(c)], causing the closure of the tension crack before being decelerated by the saturated sand mass at the slope toe. Examination of photographic evidences shows that the seepage area had already developed, as far as 5 cm above the slope toe, when the slope failed.

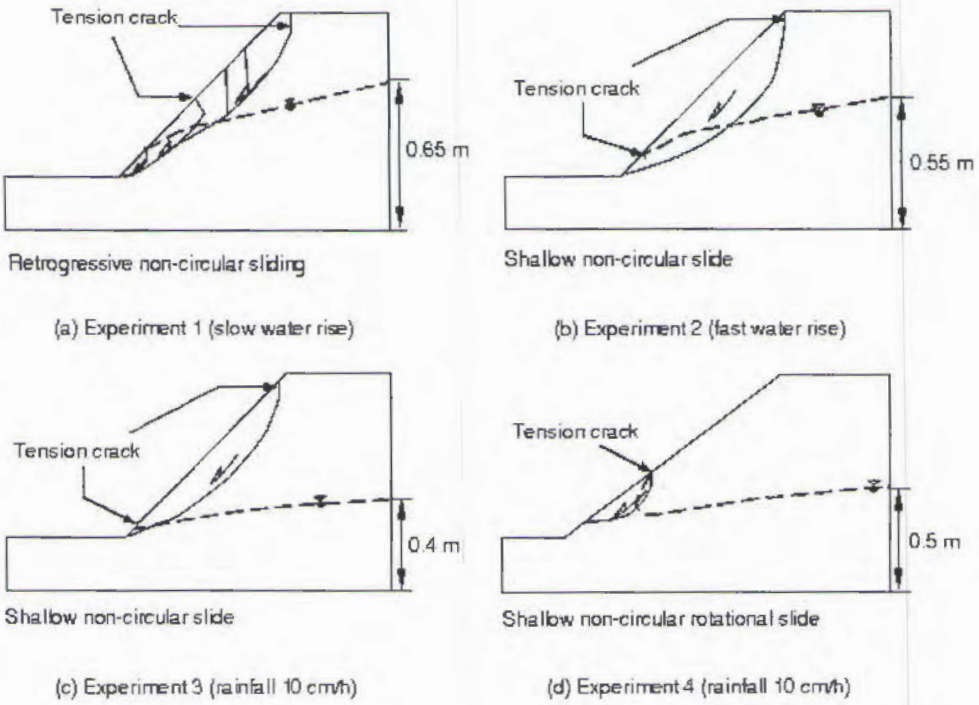

Fig. 9. Summary of failure modes in each experiment

In the residual granite soil slope (Exp. 4), a total of 200 cm of rain was required to initiate slope failures, due to the prolonged existence of entrapped air within the slope, which prevented the hydraulic conductivity of the soil to reach its saturated value. The observed slope failures occurred in two localized shallow slides, initiated 2 h after the formation of respective tension cracks. The first slide [Stage 1 in Fig. 8(d)] involved the soil mass, in the middle part of the slope, about 15 cm above the tip of the slope toe. Observational evidence indicated that the seepage area had already developed as far as 15 cm above the slope toe at the time of the initiation of failure. The uppermost boundary of the seepage area was a few centimeters below the failure crown, as indicated by water seeping from the head scarp after the failure. Stage 2 sliding occurred adjacent to the location of Stage 1, when the seepage area developed further uphill 7 h after the cessation of the previous stage of the failure. Considering the failure development, side friction had probably existed and inhibited sliding along the soil/wall interface. The large time difference between failure initiation and failure occurrence suggests the existence of apparent cohesion, probably due to the prolonged existence of soil suction, which maintained the local stability of the slope.

Failure Modes

Fig. 9 summarizes the modes of failure observed in all of the experiments. In general, model slopes in all the experiments failed by shallow noncircular sliding, involving a large portion of soil mass or localized soil mass near the slope surface. This general failure mode is consistent with that which characterizes the rainfall-induced failures of natural or manmade slopes (e.g., Harp et al. 1996; Baum and Chleborad 1999, Rahardjo 1999). Other contributing factors included the mode of water level rise and, to a considerable extent, the hydraulic conductivity of the soils controlled failure modes and the extent of failures.

A complex failure mechanism was observed in Experiment 1 [Fig. 9(a)], comprising different stages of localized sliding. Each stage of sliding corresponded to each step of water level rise. In the first three stages of failure, soil masses failed by retrogressive cracking and shallow noncircular sliding. However, the last stage of failure involved block sliding. It is interesting to note that although the failure modes consisted of different stages of sliding, all slides occurred on a single sliding surface.

In Experiments 2 and 3, a similar failure mode was observed despite the fact that modes of raising water level were different [Fig. 9(b and c)]. The continuous process of the water level rise within the slope and the formation of tension cracks above the toe of the slopes were the main reason for similar failure mode in Experiments 2 and 3. These two model slopes failed by shallow noncircular sliding preceded by the growth of tension cracks above the toe, with the sliding surface cutting across the slope toe. However, the failure surface observed in Experiment 2 was a little deeper than that of Experiment 3, due in part to the higher water level being developed within the slope.

In contrast, the model slope of residual granite soil in Experiment 4 failed by localized shallow rotational slides [Fig. 9(d)], owing to the slow slope wetting process associated with low hydraulic conductivity soil. In contrast to the work of Yoshitake and Onitsuka (1999), the failures notably did not involve the toe area, because the toe area was still unsaturated. This implies that rainfall-induced slope failures do not always initiate at the lower part of hillslopes, but rather at the seepage area developed anywhere on the hillslope surface. Field reports on rainfall-induced slope failures indicate that the failures also initiate at middle and upper portions of the hillslope (e.g., Shlemon et al. 1987; Wiezoreck 1987).

To evaluate the triggering mechanism observed during the experiments, slope stability analyses were performed using ordinary, Bishop, Janbu, and Spencer methods. Due to a complex failure mechanism observed in Experiment 1, the slope stability analyses were only performed for the model slopes of Experiments 2 to 4. The analyses were performed for the groundwater level that trig-

Table 3. Summary of Safety Factors for Model Slopes of Experiments 2–4

Experiment stages	Exp. number	Factor of safety							
		Without consideration of toe tension crack				With consideration of toe tension crack			
		Ordinary	Bishop	Janbu	Spencer	Ordiuary	Bishop	Janbu	Spencer
Start of	2	1.280	1.353	1.279	1.348	—	—	—	—
experiment	3	1.316	1.405	1.315	1.400	—	—	—	—
	4	1.254	1.294	1.254	1.291	—	—	—	—
At main	2	1.158	1.213	1.173	1.275	0.999[a]	1.047[a]	1.000[a]	1.075[a]
failure	3	1.179	1.217	1.183	1.235	1.082[a]	1.103[a]	1.080[a]	1.097[a]
	4	—	—	—	—	1.013	0.965	1.019	0.966

[a]Unsaturated soil mass above the toe tension crack.

gered the main movement in each model slope (see Fig. 8). The results of the analyses are summarized in Table 3. It should be clear that the increase of soil unit weight, due to saturation, would not reduce the stability of the model slope in Experiments 2 and 3 to a critical condition. All calculation methods show that the safety factors of the model slopes are still well above 1.20. However, when the saturated soil mass below the tension crack was considered having lost its strength, and hence, having no contribution to the stability of the slope, the analyses show that the safety factors for the unsaturated soil mass above the tension crack were not higher than 1.10. This indicates that the development of the tension crack, due to seepage pressure, reduced the stability of the model slopes to an unstable condition. Thus, the analytical results strongly support the experimental finding that the seepage triggered the slope failure in the Experiments 2 and 3.

Volumetric Soil Moisture Content at Failure

Volumetric soil moisture content records during all experiments, obtained from the four moisture sensors, are shown in Fig. 10. Throughout the experiments, volumetric moisture content of the soil slopes increased slowly with time toward a saturated value in

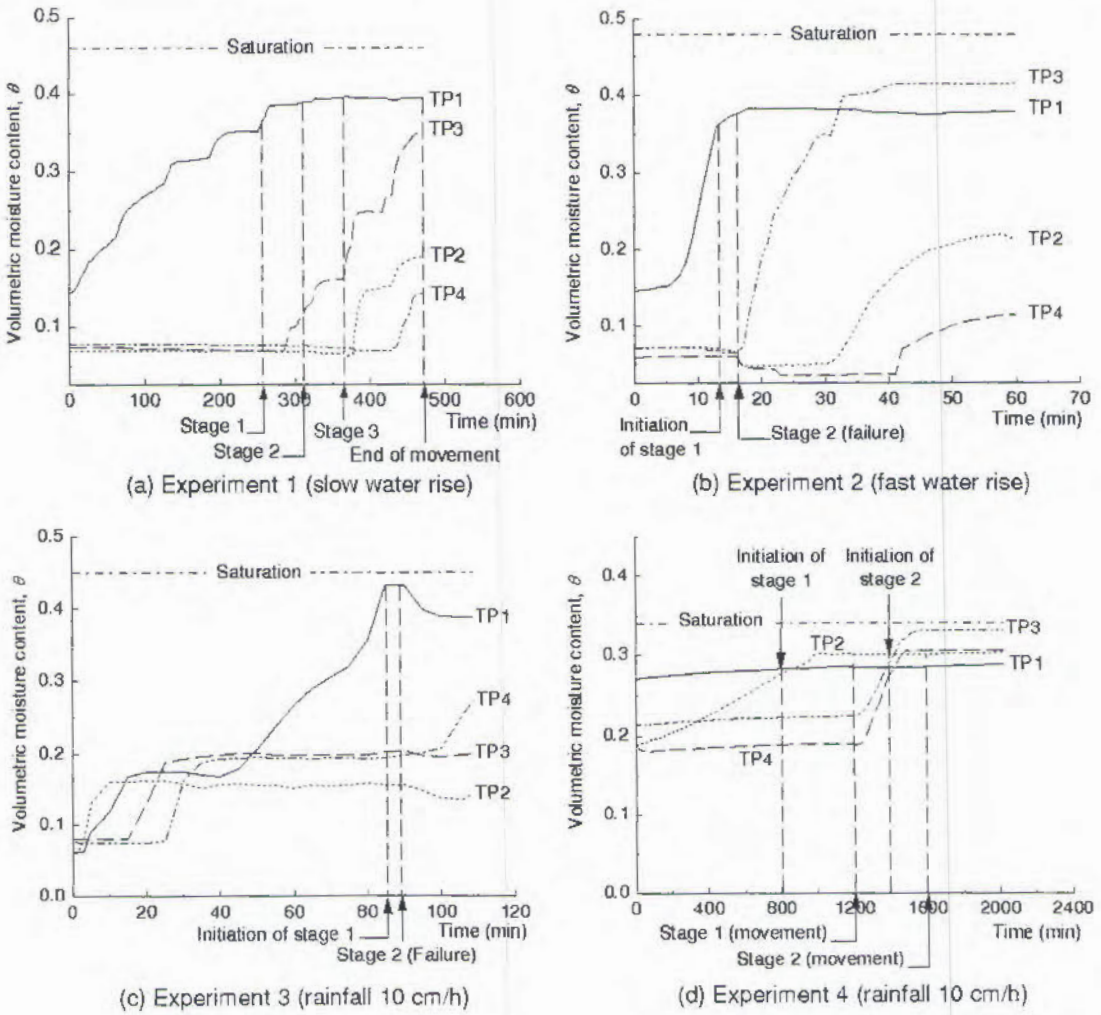

(a) Experiment 1 (slow water rise)

(b) Experiment 2 (fast water rise)

(c) Experiment 3 (rainfall 10 cm/h)

(d) Experiment 4 (rainfall 10 cm/h)

Fig. 10. Changes in soil moisture content at different stages of failure in each experiment

Table 4. Summary of Volumetric Moisture Content Records and the Corresponding Degree of Saturation

Experiment stages	Exp. number	Measured volumetric moisture content				Corresponding degree of saturation[a]			
		TP1	TP2	TP3	TP4	TP1	TP2	TP3	TP4
Start of experiment	1	0.144	0.069	0.074	0.074	31.30	15.00	16.09	16.96
	2	0.147	0.071	0.070	0.058	30.63	14.79	14.58	12.08
	3	0.062	0.067	0.081	0.075	13.78	14.09	18.00	16.67
	4	0.27	0.190	0.214	0.193	79.48	55.91	62.94	56.65
First failure initiation	1	0.353	0.067	0.088	0.076	78.26	14.57	14.78	16.52
	2	0.359	0.070	0.067	0.059	74.79	14.58	13.96	12.29
	3	0.433	0.157	0.203	0.195	96.22	34.89	45.11	43.33
	4	0.284	0.283	0.222	0.189	83.38	83.24	65.41	55.61
At first failure	1	0.360	0.067	0.068	0.070	78.26	41.57	14.78	16.52
	2	0.379	0.047	0.072	0.045	78.96	9.79	15.00	9.38
	3	0.432	0.157	0.204	0.198	96.00	34.89	45.33	44.00
	4	0.284	0.302	0.222	0.189	83.66	88.75	65.41	55.61
At end of experiment	1	0.395	0.191	0.357	0.145	85.87	41.52	77.61	31.52
	2	0.379	0.211	0.416	0.114	78.95	43.96	86.67	23.75
	3	0.388	0.146	0.200	0.274	86.22	32.44	44.44	60.89
	4	0.288	0.303	0.331	0.307	84.78	89.18	97.06	90.04

[a]Calculated values from average porosity.

response to the saturation process, during which most failures occurred. Of other factors, the hydraulic conductivity and the initial volumetric moisture content of soils clearly controlled the rate of changes in volumetric moisture content in all the experiments. It should be noted that times indicating the initiation and occurrence of movements were determined independently from the video records.

Table 4 shows the summary of the volumetric moisture content records and the corresponding calculated degree of saturation at the beginning of each experiment, failure initiation, and the end of all experiments. At the beginning of Experiments 1 and 2, the moisture sensor located just above the toe (TP1) measured higher volumetric moisture content than other sensors, since its location was closer to the initial water table. It is also obvious from Table 4 that some moisture sensors measured lower volumetric moisture content values than the calculated values (Table 1) at the end of the experiments. These differences probably resulted from the presence of entrapped air within the wet soil or the change of pore-space geometry in the wet soil npon the process of shearing.

Detailed volumetric moisture content records for all sensors, during Experiment 1, are shown in Fig. 10(a). The moisture sensor located just above the toe (TP1) clearly responded to the progressive development of seepage area at the toe. This sensor also indicated that the soil at the toe had nearly reached full saturation upon the commencement of localized toe failures (Stage 1). The next stages of water level rise extended the development of the seepage area uphill, as observed at TP1 and TP3, during which the next stages of sliding began. Other moisture sensors located near the slope surface (TP2 and TP4) still recorded low volumetric moisture content, implying that sand masses involved in the movements were still unsaturated.

In contrast, the advancing wetting front resulted, initially, in the significant rapid increase of volumetric moisture content throughout Experiment 2 [Fig. 10(b)]. Volumetric moisture content records of the toe sensor TP1 show that the volumetric moisture content of the soil at the toe had nearly reached its saturated value at the initiation of toe failure and the occurrence of the subsequent overall failure. However, the slab of sand mass, involved in the overall failure, was still unsaturated as indicated by the moisture records of near-surface sensors TP2 and TP4. Those moisture sensors also detected a distinct drop in volumetric moisture content, corresponding to a change of the volume of wet sand near those sensors, owing to shearing. Close examination of the photographic records suggests that the movement displaced not only the soil particles but also the pore water. The moisture records of TP3 show no increase or decrease in volumetric moisture content when the movement took place. This indicates that the water table was still far below the sliding soil mass, and that the sliding surface was well above the sensor TP3.

Fig. 10(c) shows the volumetric moisture content records during Experiment 3. Well-distributed initial volumetric moisture content was observed in the river sand slope, as indicated by all moisture sensors (θ=0.08). The first stage of increase in volumetric moisture content was very prominent near the slope surface at the beginning of the experiment, with the shallower sensors (TP1 and TP2) responding earlier than those deeper within the slope profile. The sensor located just above the slope toe (TP1) recorded the next stage of increase in moisture content, that led to the initiation of Stage 1 movement in the toe vicinity. The moisture records of TP1 show that the soil at the toe reached a nearly-saturated condition, when the Stage 2 movement occurred. It should be emphasized that this movement involved, mainly, the soil near the slope surface; and it is evident from moisture records of the near-surface sensor TP2 that the major portion of the sliding sand mass was still, considerably, unsaturated. In addition, moisture sensors located within the failed sand mass (TP1–TP3) measured a distinct volumetric moisture content drop after Stage 2 movement, probably due to the reduction in the volume of the sand involved in the movement, with a larger reduction occurring in the saturated toe area (TP1).

The changes in volumetric moisture content in Experiment 4 are presented in Fig. 10(d). The calculated initial saturation of the soil throughout the slope profile varied approximately from 50 to 80% (Table 4). The volumetric moisture content records indicate that the soil close to the slope base to be significantly more saturated than the rest of the slope area. The infiltration of rainwater induced an increase in volumetric moisture content in most parts of the soil slope. However, the infiltration process was slower